Analysis of coupling between hydrodynamic and thermal instabilities in non-Boussinesq convection

Sergey A. Suslov

Department of Mathematics and Computing, University of Southern Queensland, Toowoomba, Queensland 4350, Australia.
E-mail: ssuslov@usq.edu.au

Abstract

High temperature convection arises in many technical applications such as thermal insulation systems, chemical vapour deposition reactors etc. Under high temperature conditions fluid density and transport property variations can reach up to 30% of the average values across the flow region. Associated symmetry breaking nonlinearities are responsible for a wide spectrum of flow instabilities not found in low temperature flows that are typically described by the Boussinesq approximation of the Navier-Stokes equations. In this work we use a set of Low-Mach number equations suggested by Paolucci in the early 1980's to describe a high-temperature mixed convection flow between two vertical plates. We find that non-Boussinesq instabilities have either a hydrodynamic (shear, common to both low- and high- temperature flows) or thermal (buoyancy, purely non-Boussinesq) character and they can occur simultaneously at certain values of the governing physical parameters (the so-called codimension-2 points). We use a weakly nonlinear analysis to show that such situations can be successfully modelled by two coupled cubic complex Landau equations. Subsequently the unfoldings of the double Hopf bifurcations involving shear modes detected in weakly non-Boussinesq mixed convection are investigated, and the complete set of resulting flow patterns is then studied as functions of the governing parameters. The spatio-temporal competition between shear and buoyancy disturbances in a strongly non-Boussinesq regime is also modelled by two coupled complex Ginzburg-Landau equations. The results obtained for these model equations are then interpreted from the physical point of view and the nature and asymptotic outcomes of instability mode competition at large times are discussed.

Introduction and problem definition

Consider a flow of air with the average (reference) temperature $T_r = 300K$ whose density ρ, dynamic viscosity μ, thermal conductivity k and specific heat

Article published in Nonlinear Analysis 63(5) (2005) 1435–1443

c_p nondimensionalised with respect to their values at T_r vary with temperature T according to the ideal gas and Sutherland formulae

$$\rho T = P, \quad \mu = T^{3/2}\frac{1.368}{T+0.368}, \quad k = T^{3/2}\frac{1.648}{T+0.648}, \quad c_p = 1 \tag{1}$$

between two very long vertical plates separated by the gap of width H forming either a long open channel or a tall cavity. The plates are isothermal and maintained at different temperatures T_h and T_c, $T_h > T_c$. As discussed in Suslov and Paolucci (1995) such flow is described by the Low-Mach-Number equations

$$\frac{\partial \rho}{\partial t} + \frac{\partial \rho u_i}{\partial x_i} = 0\,, \tag{2}$$

$$\frac{\partial \rho u_i}{\partial t} + \frac{\partial \rho u_i u_j}{\partial x_j} = -\frac{\partial \Pi}{\partial x_i} + \frac{Gr}{2\epsilon}(\rho - 1)n_i + \frac{\partial \tau_{ij}}{\partial x_j} \tag{3}$$

$$\rho c_p \left(\frac{\partial T}{\partial t} + u_j \frac{\partial T}{\partial x_j}\right) = \Gamma \frac{dP}{dt} + \frac{1}{Pr}\frac{\partial}{\partial x_j}\left(k\frac{\partial T}{\partial x_j}\right)\,, \tag{4}$$

where the Grashof, Reynolds and Prandtl numbers, non-dimensional temperature difference ϵ between the walls and the fluid resilience parameter Γ are defined as

$$Gr = \frac{\rho_r^2 g(T_h - T_c)H^3}{\mu_r^2 T_r},\ Re = -\frac{\rho_r H^3}{12\mu_r^2}\frac{d\Pi}{dy},\ \epsilon = \frac{T_h - T_c}{2T_r},\ Pr = \frac{\mu_r c_{pr}}{k_r} = 0.71,\ \Gamma = \frac{2}{7}\,.$$

The thermodynamic pressure $P \equiv 1$ for an open channel or is determined by the global mass conservation $\int_V \rho\, dV = 1$ for a closed cavity, respectively. The primary steady parallel flow is driven by buoyancy forces (natural convection in a cavity), the applied longitudinal pressure gradient (forced convection in a channel) or by their combination (mixed convection in a channel). Here we investigate in detail two representative regimes: (I) mixed convection in a channel at $(Gr_{\rm I}, Re_{\rm I}, \epsilon_{\rm I}) = (5269212, -5179, 0.3)$ and (II) natural convection in a cavity at $(Gr_{\rm II}, Re_{\rm II}, \epsilon_{\rm II}) = (16900, 0, 0.6)$. Nonlinear fluid property variations (up to 30%) with temperature play a symmetry breaking role and result in the appearence of multiple instability modes not found in the classical Boussinesq formulation. Here we endeavour to understand the mechanism of their interactions.

Codimension-2 unfoldings in regime (I)

A linear stability analysis of steady parallel basic flow in this regime is summarized in Fig. 1; it reveals that the marginal stability curve $Gr(Re)$ has a kink singularity and both critical wave number α and critical disturbance wave speed c are discontinuous. The real leading disturbance amplification rate curve $\sigma^R(\alpha)$ shown for this regime by the plain solid line in Fig. 1(d) has a peculiar shape as well: it has two zero maxima at wavenumbers $\alpha_1 = 0.0795$

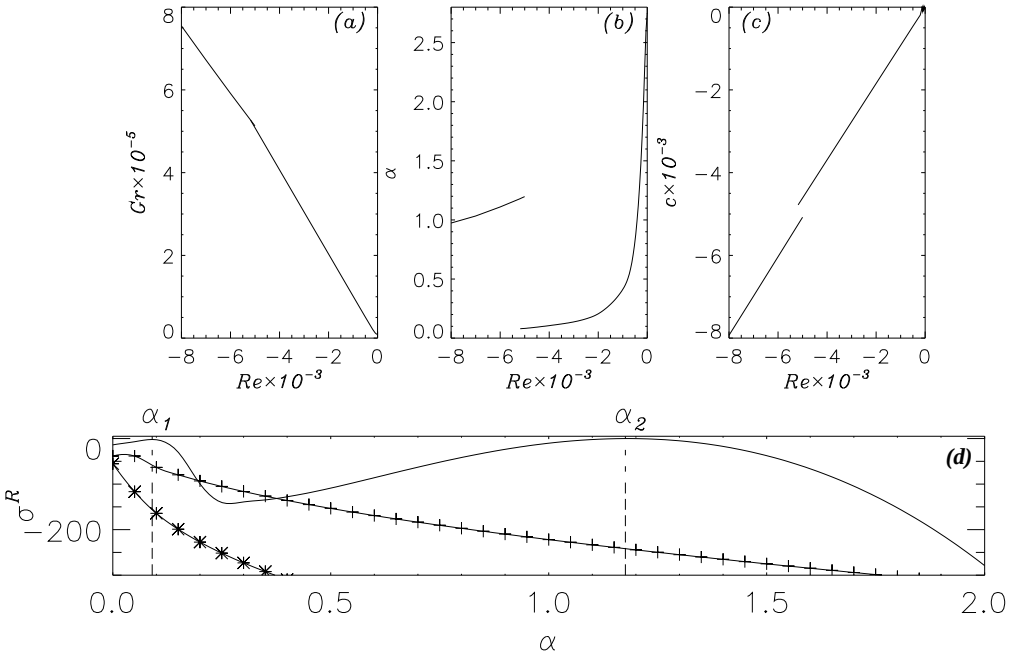

Fig. 1. Linear stability diagram and the disturbance amplification rates in regime (I).

and $\alpha_2 = 1.1804$. This is the so-called codimension-2 point. Depending on the values of physical parameters in the vicinity of $(Gr_{\rm I}, Re_{\rm I}, \epsilon_{\rm I})$ either left or right maximum crosses the zero level first. The resulting flow pattern depends on the nonlinear interaction of two disturbance wave envelopes centered at wavenumbers α_1 and α_2 shown by vertical dotted lines in Fig. 1(d). Both disturbance wave envelopes belong to the same branch of the problem dispersion relation. Hence they have the same physical nature, namely, the shear which has maximum near the inflection point of the basic flow velocity profile. This is consistent with conclusions made in Suslov and Paolucci (1995), but at that time it was overlooked that the instability was caused by the same shear mode (switching the wavenumber) rather than by two distinct modes. The asymptotic behaviour of the system is determined by the relatively narrow neighborhoods of α_1 and α_2 for which the temporal amplification rate σ^R is positive. Since α_1 and α_2 are well separated from each other, in the context of further derivation we consider the corresponding wave envelopes to be independent but subject to weakly nonlinear interaction. The systematic disturbance amplitude expansion about the basic flow solution introduced in Suslov and Paolucci (1997b) and adapted to the codimension-2 analysis in Suslov and Paolucci (1997a) is truncated to third order in amplitudes $A_1(t)$ and $A_2(t)$ corresponding to the disturbances with wavenumbers α_1 and α_2, respectively, and reads

$$\mathbf{w} = \mathbf{w}_{000} + |A_1|^2\mathbf{w}_{200}^{(1)} + |A_2|^2\mathbf{w}_{200}^{(2)} + \tag{5}$$
$$\Big\{\Big[A_1\left(\mathbf{w}_{110} + |A_1|^2\mathbf{w}_{310}^{(1)} + |A_2|^2\mathbf{w}_{310}^{(2)}\right)E_1 + A_1^2\mathbf{w}_{220}E_1^2 + A_1A_2^*\mathbf{w}_{21-1}E_1E_2^* +$$
$$A_2\left(\mathbf{w}_{101} + |A_1|^2\mathbf{w}_{301}^{(1)} + |A_2|^2\mathbf{w}_{301}^{(2)}\right)E_2 + A_2^2\mathbf{w}_{202}E_2^2 + A_1A_2\mathbf{w}_{211}E_1E_2\Big] + \text{c.c.}\Big\},$$

where $\mathbf{w} = (u, v, T, \Pi)^T$, the first index corresponds to the order of amplitude, the second and the third ones to the powers of $E_1 = \exp(i\alpha_1 y)$ and $E_2 = \exp(i\alpha_2 y)$. The asterisk and c.c. denote complex conjugate. In order for (5) to satisfy equations (1)–(4) the evolution of disturbance amplitudes should be governed by a system of the coupled Landau equations

$$\frac{da_j}{dt} = a_j \left(\sigma_j^R + K_{j1}^R a_1^2 + K_{j2}^R a_2^2\right), \qquad \frac{d\theta_j}{dt} = \sigma_j^I + K_{j1}^I a_1^2 + K_{j2}^I a_2^2, \tag{6}$$

where $A_j = |A_j| \exp(\mathrm{i}\theta_j) = a_j \exp(\mathrm{i}\theta_j)$, $\sigma_j = \sigma^R + i\sigma^I$ are the eigenvalues of the linearised problem and $K_{jk} = K_{jk}^R + \mathrm{i}K_{jk}^I$, $j, k = 1, 2$ are the complex Landau coefficients determined by the orthogonality conditions Suslov and Paolucci (1997b)

$$\langle \mathbf{w} - \mathbf{w}_{000} - A_j \mathbf{w}_{1(2-j)(j-1)}, \mathbf{w}_{1(2-j)(j-1)} \rangle = 0.$$

All coefficients in the above system depend on physical governing parameters thus making analysis of the codimension-2 dynamics a nontrivial task.

Consider the two amplitude equations (6) which are completely decoupled from the pair of the phase equations. Using transformations

$$r_1 = a_1 \sqrt{|K_{11}^R|}, \quad r_2 = a_2 \sqrt{|K_{22}^R|}, \quad \mu_1 = -\sigma_1^R, \quad \mu_2 = -\sigma_2^R,$$
$$b = -\frac{K_{12}^R}{|K_{22}^R|}, \quad c = -\frac{K_{21}^R}{|K_{11}^R|}, \quad d = -\frac{K_{22}^R}{|K_{22}^R|}, \quad t \to -t$$

we reduce the amplitude equations (6) to the canonical form

$$\dot{r}_1 = r_1 \left(\mu_1 + r_1^2 + b r_2^2\right), \quad \dot{r}_2 = r_2 \left(\mu_2 + c r_1^2 + d r_2^2\right) \tag{7}$$

which has been analysed in Guckenheimer and Holmes (1985). Numerical evaluation of the above coefficients at $(Gr_{\mathrm{I}}, Re_{\mathrm{I}}, \epsilon_{\mathrm{I}})$ results in $b = 0.925$, $c = -67.340$, $d = 1$, $\mu_1 = \mu_2 = 0$ which corresponds to Type 2a case II of the fixed point with three invariant lines $\left(r_1 = 0, r_2 = 0, \; r_2 = \sqrt{\frac{1-c}{d-b}} r_1\right)$ according to the classification given in Guckenheimer and Holmes (1985), Tables 7.5.1 and 7.5.2. In order to unfold this bifurcation note that the four types of equilibria (r_{1e}, r_{2e}) are possible in system (7): a) linearly stable basic flow, (0,0); b) and c) individually bifurcating modes $(\sqrt{-\mu_1}, 0)$ and $\left(0, \sqrt{-\mu_2/d}\right)$; and d) interacting modes $\left(\sqrt{\frac{b\mu_2 - d\mu_1}{d-bc}}, \sqrt{\frac{c\mu_1 - \mu_2}{d-bc}}\right)$. Stability of the above fixed points is determined by the eigenvalues $\lambda_{1,2}$ of a problem obtained by linearizing equations (7) about the equilibrium ($\lambda_{1,2}^R > 0$ for stability because of the time reversion):

$$\lambda_{1,2} = \frac{C_{11} + C_{22}}{2} \pm \frac{1}{2}\sqrt{16bcr_{1e}^2 r_{2e}^2 + (C_{11} - C_{22})^2}, \qquad \begin{array}{l} C_{11} = \mu_1 + 3r_{1e}^2 + br_{2e}^2 \\ C_{22} = \mu_2 + 3dr_{2e}^2 + cr_{1e}^2 \end{array}.$$

When $d = 1$ the stability conditions for equilibria a)–d) are: a) μ_1, $\mu_2 > 0$; b) $\mu_2 > c\mu_1$; c) $\mu_1 > b\mu_2$; and d) is always stable if it exists. Consequently, unfoldings of the codimension-2 point are determined by lines $\mu_1 = 0$, $\mu_2 = 0$,

$\mu_2 = c\mu_1$ and $\mu_1 = b\mu_2$. All topologically distinct amplitude flow diagrams near the considered codimension-2 point are presented in Fig. 2. Straight lines $a_1 = 0$, $a_2 = 0$ and $a_2 = a_1\sqrt{\frac{K_{11}^R - K_{21}^R}{K_{22}^R - K_{12}^R}} \approx 1.319 a_1$ in plot (1) are the invariant lines at the codimension-2 point $(Gr_{\rm I}, Re_{\rm I})$. The third of these lines is algebraically attractive so that the distance between it and the trajectories decreases asymptotically as $t^{-3/2}$ while the evolution along the invariant line towards the origin is $a_1 \sim a_2 \sim t^{-1/2}$. Plots (2)–(7) show all possible unfoldings of a fixed point for case II in Guckenheimer and Holmes (1985). These unfoldings are not discussed in Guckenheimer and Holmes (1985) and thus complement the general classification of codimension-2 points given there. The middle plot in Fig. 2 relates the unfoldings to the physical parameter space for non-Boussinesq mixed convection.

In order to complete the analysis the phase evolution given by the second pair of equations (6) has to be considered. In particular, the possibility of the phase locking as well as resonances needs to be examined. The phase locking condition is

$$\sigma_1^I - \sigma_2^I + \left(K_{11}^I - K_{21}^I\right) a_1^2 + \left(K_{12}^I - K_{22}^I\right) a_2^2 = 0\,. \tag{8}$$

Differentiating it with respect to time and using (6) after some algebra we conclude that (8) may be satisfied only if both amplitudes are constant, i.e. at the stable mixed fixed points $a_{1e}a_{2e} \neq 0$ existing in between the dash-dotted lines in Fig. 2 (see plots (4) and (5) for the flow topology). Condition (8) then becomes

$$\frac{\left(K_{11}^I - K_{21}^I\right)\left(\sigma_2^R K_{12}^R - \sigma_1^R K_{22}^R\right) + \left(K_{12}^I - K_{22}^I\right)\left(\sigma_1^R K_{21}^R - \sigma_2^R K_{11}^R\right)}{K_{11}^R K_{22}^R - K_{12}^R K_{21}^R} = \sigma_2^I - \sigma_1^I\,,$$

but it is not satisfied anywhere in Fig. 2. Finally, the ratio σ_2^I/σ_1^I remains between 16 and 17 for all points in Fig. 2. Therefore no strong resonances occur and the performed analysis accounting for the evolution of amplitudes is sufficient.

Now we relate the unfolding results to the physical flow in regime (I). As mentioned in the introduction the flow is influenced by two competing effects: the buoyancy force and the pressure gradient applied along the channel. Shear driven instability occurs near the inflection point of the basic flow velocity profile. This inflection point is due to the action of the buoyancy forces and appears only if the ratio $Gr/|Re|$ is sufficiently large. For this reason the critical Grashof number increases rapidly with $|Re|$ as seen from Fig. 1 (a). At the nearly zero values of $|Re|$ (small pressure gradient) the instability is characterised by almost stationary rolls appearing near the inflection point of the basic velocity profile with the wavelength $\lambda = 2\pi H/\alpha \approx 2.3H$ (Fig. 1 b). As the driving pressure gradient increases these rolls start drifting downwards with the primary flow and elongate. Thus the pressure gradient has a stretch-

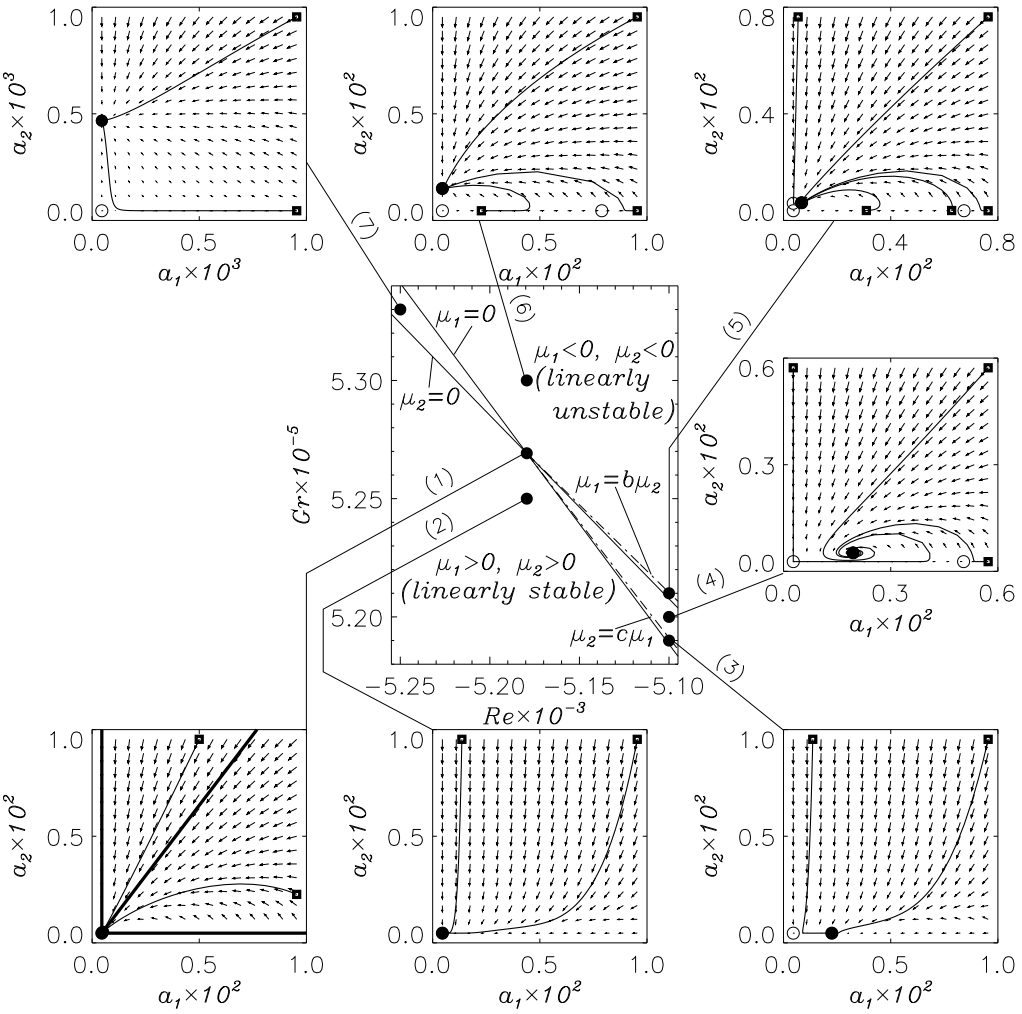

Fig. 2. Amplitude flow diagrams and trajectories near the codimension-2 point. Squares and empty and filled circles represent initial conditions and unstable and stable equilibria, respectively.

ing effect on the flow instability structures. This stretching continues until the size of rolls becomes so large that they start blocking the primary flow too strongly. At the codimension-2 point these very long instability rolls with $\lambda \approx 79H$ break into smaller ones with $\lambda \approx 5.3H$ which drift with a larger wave speed (see Fig. 1 c) and their "blocking" effect is weaker. Note that such a transition between the flow patterns is not caused by the secondary instability of the long rolls, but is rather due to a competition between the two distinct flow structures one of which drains the energy from the other. This competition is illustrated in Fig. 2. For any fixed $Re > Re_{\mathrm{I}}$ the basic flow (plot (2)) first becomes unstable due to the long wave disturbances (plot (3)), which trigger their own distortion at the slightly higher values of Gr (plot (4)). This distortion is supported by draining the energy from the long cells to finer structures (because $K_{21}^R > 0$ and $K_{12} < 0$) through the nonlinear interaction. At even higher values of Gr the shorter rolls become self-supporting

by draining the energy from the basic flow (σ_2^R becomes positive in plot (5)) and eventually destroy the long rolls completely (plot (6)). For $Re < Re_{\rm I}$ the short wave instability structures always dominate and long rolls cannot be seen (plots (2), (7) and (6)).

Spatio-temporal mode competition in regime (II)

Regime (II) corresponds to the parallel steady natural convection flow in a tall vertical enclosure which is destabilised by the simultaneous action of the physically distinct buoyancy and shear driven instability modes (Suslov and Paolucci, 1997b). Of major interest here is the spatio-temporal dynamics of localized disturbances induced by the flow turning effects of distant top and bottom ends. This is in contrast to the temporal dynamics of plain wave disturbances observed in regime (I) in an infinitely long channel. In order to include spatial modulation, expansion (5) is extended to include terms $\frac{\partial A_1}{\partial y}\mathbf{w}_{210}$, $\frac{\partial A_2}{\partial y}\mathbf{w}_{201}$, $\frac{\partial^2 A_1}{\partial y^2}\mathbf{w}^{(3)}_{310}$ and $\frac{\partial^2 A_2}{\partial y^2}\mathbf{w}^{(3)}_{301}$, where amplitudes A_i, $i = 1, 2$ become weak functions of y as well as t. The resulting weakly nonlinear evolution then is described by two coupled complex Ginzburg-Landau equations (CGLE)

$$\frac{\partial A_1}{\partial t} + c_{g1}\frac{\partial A_1}{\partial y} = \left(\sigma_1 + K_{12}|A_2|^2\right) A_1 + M_1\frac{\partial^2 A_1}{\partial y^2} + K_{11}A_1|A_1|^2\,, \tag{9}$$

$$\frac{\partial A_2}{\partial t} + c_{g2}\frac{\partial A_2}{\partial y} = \left(\sigma_2 + K_{21}|A_1|^2\right) A_2 + M_2\frac{\partial^2 A_2}{\partial y^2} + K_{22}A_2|A_2|^2\,, \tag{10}$$

where the disturbance group speeds are $c_{gi} = \mathrm{i}\frac{\partial \sigma_i}{\partial \alpha}$ and $M_i = -\frac{1}{2}\frac{\partial^2 \sigma_i}{\partial \alpha^2}$. This system of equations models local nonlinear coupling between two wave envelopes propagating with different group speeds. In regime (II) the numerical values of coefficients for the buoyancy mode at $\alpha_1 \approx 0.857$ are $\sigma_1 \approx (3.57, 95.8)$, $c_{g1} \approx -87.3$, $K_{11} \approx (-74.7, -359.5)$ and $M_1 \approx (28.8, 9.42)$ and the shear mode constants evaluated at $\alpha_2 \approx 2.580$ are $\sigma_2 \approx (4.52, 111.5)$, $c_{g2} \approx -20.3$, $K_{22} \approx (1.02 \times 10^3, -6.58 \times 10^3)$ and $M_2 \approx (22.1, -1.59)$. The mode coupling coefficients are $K_{12} \approx (-1.02 \times 10^4, 8.52 \times 10^3)$ and $K_{21} \approx (59.3, 532.1)$. It can be shown that the linearised version of the above equations has solutions which grow exponentially with real amplification rate $\sigma_i^R > 0$ when they are observed in a frame moving with the corresponding group speed. On the other hand the asymptotic amplification rates of these solutions at any fixed spatial location are given by $\sigma_i^R - c_{gi}M_i^R/\left(4|M_i|^2\right)$ which are negative in regime (II). Thus while the localized disturbances grow as they propagate downwards, they decay asymptotically at any fixed location. This situation is known as convective instability. The numerical solution of the nonlinear coupled equations (9)–(10) with boundary conditions $A(t, 0) = A(t, L) = 0$ which mimic the absorbing influence of the end walls is presented in Fig. 3.

Convectively unstable wave envelopes of buoyancy and shear disturbances interact only for a short time since they have very different group speeds and propagate in a finite domain bounded by the absorbing walls (see snapshot for $t = 0.04$ and $t = 0.20$). During this nonlinear interaction phase the energy is transfered from the buoyancy to shear mode as indicated by the signs of the corresponding coupling coefficients K_{ij}^R, $i \neq j$. The wave envelopes induced by the initial pulses near the bottom of the cavity and seen for $t = 0.4$ remain there as they are swept towards that wall with their negative group speed. Because of the convective character of instability the extension rate of these wave packets is not sufficiently large to overcome their drift and they decay quickly due to the absorbing influence of the nearby wall. They are not seen at $t = 0.32$. The wave envelopes induced near the top of the cavity propagate downwards and spread but never occupy the whole cavity as they are only convectively unstable (see snapshot at 0.32). The wave envelopes corresponding to the buoyancy and shear modes are clearly distinguished for $t = 0.32$ by very different wavelengths. The buoyancy disturbance envelope moves faster and decays after it reaches $y = 0$ emphasizing the convective nature of this instability and absorbing boundary conditions (compare snapshots for $t = 0.32$ and 0.68). The long term behaviour of the shear mode amplitude is essentially different. The initial envelope breaks into several parts and loses its symmetry as it hits $y = 0$: the wave amplitude is generally larger near $y = 0$ towards which the envelope propagates. The shear disturbance amplitude tends to zero near $y = L$ once again demonstrating the linearly convective character of instability of this mode. Nevertheless, unlike the buoyancy mode, the shear disturbances never decay even after reaching the bottom wall. This is because of the subcritical nature of the corresponding bifurcation ($K_{22}^R > 0$): by the time the shear envelope reaches the bottom of the cavity it has a magnitude larger than a threshold value of $A_{th} = \sqrt{\sigma_2^R / K_{22}^R} \approx 0.067$ so that the nonlinear destabilization becomes sufficiently strong to maintain shear instability.

The corresponding DNS results are also presented in Fig. 3 and are consistent with the CGLE predictions. After the parallel basic flow is established in the middle part of the cavity by time $t = 0.13$, a large buoyancy disturbance starts propagating from the top end of the cavity. Its wavenumber is approximately 0.96 which is just slightly larger than α_1 predicted by linear analysis. Since the $\sigma_2^R > 0$, the flow is linearly unstable with respect to shear disturbances which are seen as shorter waves at $t = 0.87$ and $t = 2.15$. The two instability modes interact at larger times resulting in a somewhat irregular flow pattern ($t = 0.87$). Eventually, the convectively unstable buoyancy disturbance reaches the bottom wall and decays while the slower propagating shear disturbances form the pattern seen in the upper part of the snapshot at $t = 2.15$. This snapshot agrees qualitatively with the numerical solution of CGLE for $t = 1.40$ shown in Fig. 3: with a regular periodic tail and irregular head of the resulting wave envelope.

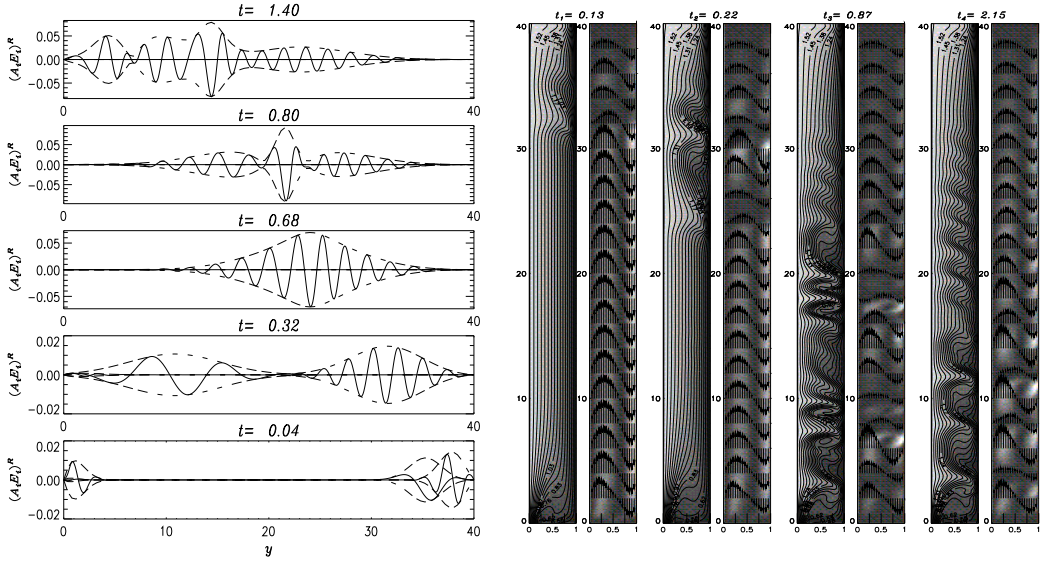

Fig. 3. Solutions of the coupled equations (9)–(10) (horizontal plots) and DNS flow fields (vertical plots) in regime (II). Lighter regions in thermal (left) and velocity (right) fields correspond to higher temperature and larger kinetic energy, respectively.

The two multi-mode interacting instability regimes studied here demonstrate the wealth of flow patterns which are observed in realistic fluids subject to large temperature gradients. The results presented here are far beyond the reach of the standard Boussinesq treatment which has been used in majority of convection studies to date.

References

Guckenheimer, J., Holmes, P., 1985. Nonlinear Oscillations, Dynamical Systems, and Bifurcations of Vector Fields. Springer-Verlag.

Suslov, S. A., Paolucci, S., 1995. Stability of mixed-convection flow in a tall vertical channel under non-Boussinesq conditions. J. Fluid Mech. 302, 91–115.

Suslov, S. A., Paolucci, S., 1997a. Non-Boussinesq convection in a tall cavity near the codimension-2 point. In: Ulucakli et al., M. E. (Ed.), Proceedings of the ASME Heat Transfer Division. Vol. 3, HTD-353. ASME Press, pp. 243–250.

Suslov, S. A., Paolucci, S., 1997b. Nonlinear analysis of convection flow in a tall vertical enclosure under non-Boussinesq conditions. J. Fluid Mech. 344, 1–41.